Received: 26 July 2019 | Revised: 18 January 2020 | Accepted: 21 January 2020

DOI: 10.1002/mrm.28211

NOTE

Magnetic Resonance in Medicine

A within-coil optical prospective motion-correction system for brain imaging at 7T

Phillip DiGiacomo[1] | Julian Maclaren[2] | Murat Aksoy[2] | Elizabeth Tong[2] | Mackenzie Carlson[1] | Bryan Lanzman[2] | Syed Hashmi[2] | Ronald Watkins[2] | Jarrett Rosenberg[2] | Brian Burns[3] | Timothy W. Skloss[4] | Dan Rettmann[5] | Brian Rutt[1,2] | Roland Bammer[6] | Michael Zeineh[2]

[1]Department of Bioengineering, Stanford University, Stanford, California

[2]Department of Radiology, Stanford University, Stanford, California

[3]Applied Sciences Lab West, GE Healthcare, Menlo Park, California

[4]MR Advanced Systems, GE Healthcare, Waukesha, Wisconsin

[5]MR Applications and Workflow, GE Healthcare, Rochester, Minnesota

[6]Department of Radiology, University of Melbourne, Melbourne, Australia

Correspondence
Michael Zeineh, Department of Radiology, Stanford University, 1201 Welch Road, Rm P271, Stanford, CA 94305.
Email: mzeineh@stanford.edu

Funding information
Foundation of the American Society of Neuroradiology, Grant/Award Number: Boerger Alzheimer's Fund; National Institutes of Health, Grant/Award Number: P41 EB015891, S10 RR026351-01A1, R01 AG061120-01; GE Healthcare

Purpose: Motion artifact limits the clinical translation of high-field MR. We present an optical prospective motion correction system for 7 Tesla MRI using a custom-built, within-coil camera to track an optical marker mounted on a subject.

Methods: The camera was constructed to fit between the transmit–receive coils with direct line of sight to a forehead-mounted marker, improving upon prior mouthpiece work at 7 Tesla MRI. We validated the system by acquiring a 3D-IR-FSPGR on a phantom with deliberate motion applied. The same 3D-IR-FSPGR and a 2D gradient echo were then acquired on 7 volunteers, with/without deliberate motion and with/without motion correction. Three neuroradiologists blindly assessed image quality. In 1 subject, an ultrahigh-resolution 2D gradient echo with 4 averages was acquired with motion correction. Four single-average acquisitions were then acquired serially, with the subject allowed to move between acquisitions. A fifth single-average 2D gradient echo was acquired following subject removal and reentry.

Results: In both the phantom and human subjects, deliberate and involuntary motion were well corrected. Despite marked levels of motion, high-quality images were produced without spurious artifacts. The quantitative ratings confirmed significant improvements in image quality in the absence and presence of deliberate motion across both acquisitions ($P < .001$). The system enabled ultrahigh-resolution visualization of the hippocampus during a long scan and robust alignment of serially acquired scans with interspersed movement.

Conclusion: We demonstrate the use of a within-coil camera to perform optical prospective motion correction and ultrahigh-resolution imaging at 7 Tesla MRI. The

setup does not require a mouthpiece, which could improve accessibility of motion correction during 7 Tesla MRI exams.

KEYWORDS

neuroimaging, optical motion correction, prospective motion correction, ultrahigh field MRI

1 | INTRODUCTION

Ultrahigh-field (7 Tesla [T]) MRI systems can produce images with higher SNR and spatial resolution than lower-field strength MR systems (1.5T, 3T). In recent years, ultrahigh-field MRI has been used to elucidate novel insights into the pathology of neurological and neuropsychiatric diseases ex vivo.[1-4] These findings have led to a growing number of in vivo studies performed at 7T, for which increased resolution of structural and functional scans has led to enhanced visualization of microstructures[5,6] and novel networks of brain connectivity,[7] enabling insights into the pathology of a range of neurological diseases.[8-13] However, achieving both high SNR and high resolution requires long scan times. Although work is currently being done to accelerate scans at 7T,[14] the requisite long scan times often result in image artifacts due to subject motion. These motion artifacts limit the clinical interpretability of images and the reliability of quantitative analyses, such as segmentations that estimate volume and thickness. For these reasons, it is critical to prevent or correct for motion artifact in 7T MR images, particularly those acquired at very high resolution, to identify and develop novel imaging-based biomarkers of disease.

Retrospective methods for motion correction are available[15-17] but require longer postprocessing time and may be insufficient due to overlaps and gaps in k-space.[18] Prospective motion correction can overcome this limitation using measured head position and orientation to update the imaging volume position and orientation within the bore in real time. The necessary real-time head pose information can be obtained using several techniques, including active markers,[19] field probes,[20,21] real-time navigator acquisitions,[22] or optical tracking using a camera system.[23,24] In the latter case, because the camera is independent of the MRI scanner, application to most clinical sequences is possible with real-time adjustment of k-space trajectories. Prior work has shown that prospective motion correction (PMC) systems can enable higher resolution structural imaging in volunteers than would otherwise be achievable[25,26] and can provide improved quantitative susceptibility maps.[27]

Despite these promising results, 1 obstacle that remains in translating optical PMC to high-field MRI and routine clinical use is maintaining sufficiently clear line of sight from the camera to a head-mounted optical marker. Early proof-of-concept studies used multiple cameras external to the bore of the MRI scanner,[28,29] making line of sight for long- or narrow-bore magnets, enclosed head coils, or large subjects a challenge and also limiting clinical utility. The development of MR-compatible cameras has made it possible to use cameras within the B_0 field of the scanner, for example, attached to the inner surface of the bore or to a rig placed around the receive-only head coil.[24] Our prior work at 3T used a single camera mounted directly on the receive-only head coil such that an unimpeded view of an optical marker to the subject's head can be achieved between the rungs of the coil.[30,31] However, because most commercial 7T systems do not use a body RF transmit coil due to heating limitations, available head coils at 7T are typically enclosed within an RF transmit shell, making an unimpeded and reliable line of sight to a head-mounted marker a challenge, leading to the use of mouthpieces to extend marker visibility beyond the head coil at 7T.[25-27] Addressing this challenge is critical to translating the ultrahigh-resolution imaging that has been achieved using these systems to broader research and clinical use.

The present work fully addresses this challenge through the design of a slim, custom-built camera that fits between shells of Nova Medical (Nova Medical, Wilmington, MA) 32 receive (Rx) head coils (either 2-channel transmit or 8-channel transmit versions) used in 7T GE (GE Healthcare, Chicago, IL) scanners. The direct line of sight enables visualization of an optical marker on the subject's forehead. An adhesive backing provides a rigid coupling between the subject's forehead and the marker, with improved patient tolerance compared to a mouthpiece. Here, we acquire data on 7 compliant subjects to demonstrate that the resulting PMC system has the ability to detect and correct for both rigid-head and physiologic motion across various sequences (3D-IR-FSPGR and 2D-gradient echo [GRE]). Moreover, we demonstrate that this system provides the ability to obtain high-fidelity acquisitions of ultrahigh-resolution scans that are otherwise too long for clinical use. This system can also be used to robustly align serially acquired scans, with patients moving and even leaving the scanner as long as the marker remains attached in the same position. By allowing the acquisition of ultrahigh-resolution scans free from motion artifact, the use of this system at 7T in research and clinical settings is expected to facilitate the discovery of novel neuroimaging biomarkers. Parts of this study have been previously published in abstract form.[32]

2 | METHODS

2.1 | Manufacturing and hardware

A single noncommercial, MR-compatible camera was designed and built to be mounted between the transmit–receive

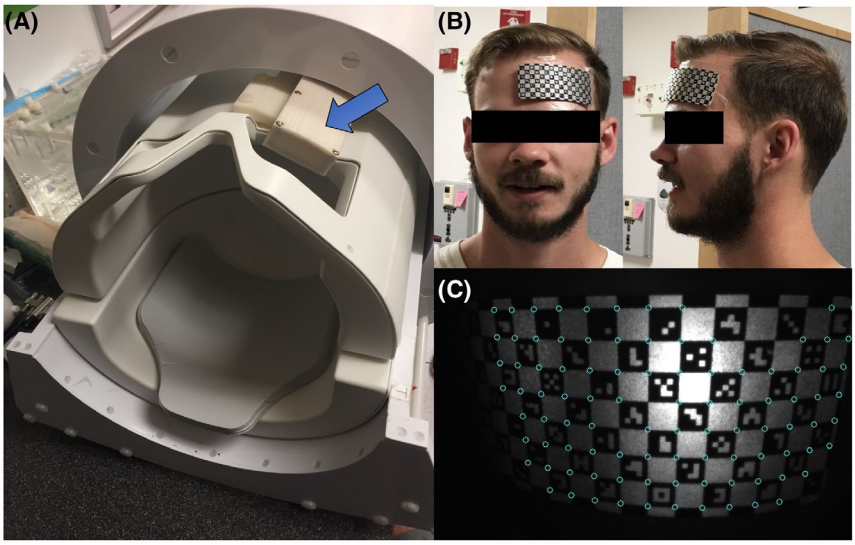

FIGURE 1 The PMC system in this study utilizes a MR-compatible camera (A) incorporated between the transmit–receive portions of the head coil to track a checkerboard optical marker (B) placed on the subject's forehead (C) for rigid tracking. Custom software identifies vertices between the barcodes to update the head position and modify gradients accordingly. PMC, prospective motion correction

shells of Nova Medical (Nova Medical) 32-channel receive head coils (either 2-channel or 8-channel transmit versions) used in 7T GE (GE Healthcare) scanners (Figure 1A). The camera prototype has a resolution of 640 × 480 and maximum frame rate of 100 Hz. The internal circuitry has been modified from our previous work at 3T MR-PET[26] to fit in the shielded, 45 mm × 144 mm assembly. This assembly is attached to a rig that mounts to the head coil (see Supporting Information Figure S1). The camera is currently powered using 2 small, nonmagnetic lithium polymer batteries, connected in series and covered in copper tape, to form a shielded 7.4V battery pack. The voltage is dropped to 5V inside the camera using a linear regulator. The battery pack is connected to the camera housing using a nonmagnetic SubMinitature version B connector, which effectively connects the shield of the camera housing to the shield of the battery. This setup gives a usable runtime of about an hour before the battery pack must be recharged, which takes roughly 30 minutes. The positioning of the camera within the coil enables direct line of sight to a checkerboard marker placed with adhesive on the left side of a subject's forehead with the subject in the typical recumbent position within the head coil (Figure 1B-C). This marker has a defined geometry, and each square on the checkerboard contains a unique barcode that allows custom software to easily identify the marker within the camera's FOV.[33] Video of the marker and plots of motion are displayed in real time. We visually assessed these and confirmed that scanning does not affect video or tracking quality. Motion correction is applied once at the beginning of each TR to avoid any delays in the sequence. The custom software determines the position of the marker and updates the scanner gradients accordingly.

2.2 | Calibration

The location of the camera within the MRI bore was calibrated as in our prior work at 3T[24] but adapted for 7T. A calibration apparatus, which incorporated wireless active markers, was built and tuned to 298 MHz. Motion was applied to the calibration apparatus, enabling a rapid (< 30 s) cross-calibration whereby the coordinate transformation between the camera and scanner coordinates was calculated. The table position in the *z*-direction is stored at the time of the calibration; thus, any change in table position (which is constantly updated by the table position encoder) relative to this initial position can be used to update the coordinate transformation. This allows the head coil to be moved synchronously with the table without losing knowledge of the camera position in the scanner reference frame.[30] This detailed calibration is needed only once. During scanning, the cross-calibration, the table position at the time of cross-calibration, and the current table position are used to continuously update the coordinate transformation.

At the beginning of each subject scan, a modified scout localizer is acquired once following landmarking to initialize the PMC system and set an initial reference point for head position. This localizer only needs to be reacquired if the marker were placed in a different position on the subject's forehead or if the table were pulled completely out such that repeat landmarking was required.

2.3 | Phantom validation

Validation to test the effect of the hardware installation on scanner stability was performed on an agar gel phantom. First, to confirm that the hardware does not cause field distortions or impact temporal stability, high-resolution EPI (1 mm × 1 mm × 3 mm resolution, 9 slices, TR = 2000 ms, TE = 30 ms, flip angle = 90, 1000 timepoints) was acquired without (twice) and with (once) the hardware installed. Then, to test whether the hardware absorbs RF energy, we measured the transmit gain and specific absorption rate accumulation during a high flip angle 2D GRE sequence (256 × 128, FOV 17, slice thickness 2.0, spacing 6.0, TE 20, TR 550, flip angle 120, bandwidth

19.23V, 1 m 14 s scan time) acquired without and with the camera hardware installed. Subsequent validation of the PMC system's motion tracking was conducted using a phantom with complex internal features (a papaya fruit). Deliberate continuous, rotational motion was applied using a wooden rod attached rigidly to the papaya during a T_1-weighted 3D-IR-FSPGR sequence (see Supporting Information Table S1 for full sequence parameters). The sequence was acquired twice, once without and once with motion correction.

2.4 | In vivo testing

2.4.1 | Subjects

Seven cooperative healthy subjects (5 female, median age of 28 years [range 25–45]) were recruited to participate in the study with approval of Stanford's Institutional Review Board and in accordance with the Health Insurance Portability and Accountability Act of 1996 after obtaining informed consent.

Imaging Protocols (Supporting Information Table S1)

1. Test 1: To test the system in vivo, the same 3D-IR-FSPGR as well as a 2D-T2-weighted oblique GRE sequence were each acquired 4 times on each subject during the same scan session: no motion with and without correction, and with motion (asked to make discrete rotations ~15 degrees to the left or right every 30 s) with and without correction. This complete protocol was run on all 7 subjects.
2. Test 2: To test the system's ability to generate high-quality ultrahigh-resolution images from otherwise untenably long acquisitions (>20 min), a 2D-GRE sequence with 4 averages was acquired on subject 1 without motion and with motion correction.
3. Test 3: Because a continuous 20-min scan is likely untenable in many clinical populations, an alternative ultrahigh-resolution, 2D-GRE acquisition was obtained by averaging a series of 4 serially acquired single average acquisitions without motion and with correction on subject 1. The subject was allowed to relax, stretch, and rotate the head between acquisitions.
4. Test 4: A fifth single average ultrahigh-resolution, 2D-GRE acquisition was acquired on subject 1 following the subject table being removed from the bore and the subject being asked to sit upright, followed by placing the subject back in the scanner. This was to assess the ability of optical prospective correction to correct for motion and changes in positioning in clinical settings when subjects may need to leave the bore (eg, to use the bathroom or take a break during scanning, both of which commonly occur clinically).

Recorded tracking data were used to quantify and calculate summary statistics of 3D translational and rotational motion for each acquisition.

2.5 | Quantitative analysis

Three blinded, experienced neuroradiologists (B.L., S.H., and M.Z. with 4, 3, and 11 years of postresidency neuroradiology experience, respectively) separately evaluated the 3D-IR-FSPGR and 2D-GRE images from test 1 for motion-related artifacts (eg, ringing, blurring, ghosting, and striping), attributing an assessment of scan quality on a 5-point scale (with a 1 representing excellent image quality and a 5 representing completely corrupted by artifact) to each acquisition based in part on previous criteria.[34] The neuroradiologists then assessed the 3D-IR-FSPGR acquisitions for visualization of the gray–white matter junction and for the 2D-GRE acquisitions for visualization of deep gray nuclei (subthalamic and red nuclei and substantia nigra) and the hippocampus, separately, on 5-point scales based in part on previous criteria.[35] These features were selected because they are of different size and contrast and are clinically relevant. Data from 2 subjects were used as test images to train the raters and reach agreement on each scale. Data from the remaining 5 subjects were then used for analysis. The order in which the datasets and sequences were presented was randomized across readers. Overall agreement among readers was high (Krippendorf's alpha coefficient = 0.89, 95% confidence interval: 0.87-0.92). The effects of deliberate motion, motion correction, their interaction, and acquisition type were tested on each scale with generalized linear regression models with log link, adjusted for clustering within subject and reader. All statistical analyses were done with Stata Release 15.1 (StataCorp LP, College Station, TX).[36] A P value less than 0.05 was considered significant.

3 | RESULTS

3.1 | Phantom validation

Validation tests performed on an agar gel phantom without and with the hardware installed showed no change in echo-planar distortion or signal variance over time (Supporting Information Figure S2A,B). Likewise, the magnitude difference maps computed between the with and without camera acquisitions (Supporting Information Figure S2C) show similar magnitude to those from duplicate acquisitions without the camera (Supporting Information Figure S2D). In the 2D-GRE experiment, the addition of the camera hardware caused an increase in transmit gain from 163 to 173 (1.0 dB), which corresponds to a 12.2% increase in transmit voltage.

We also measured a 26% increase in apparent specific absorption rate (2.3 W/kg without camera, 2.9 W/kg with camera). The papaya phantom validation study reveals a reduction in motion artifact with PMC (Supporting Information Figure S3). The uncorrected acquisition (Supporting Information Figure S3A) is heavily corrupted by artifact, limiting contrast of the fine detail of the interior, seed-containing portion of the papaya. The corrected acquisition (Supporting Information Figure S3B) shows more clearly delineated boundaries despite similar levels of motion.

3.2 | In vivo testing

1. Test 1: The 3D-IR-FSPGR (Figure 2A,C) and 2D-GRE (Figure 2E,G) images acquired without deliberate rotational motion display modest levels of translational (<2 mm) and rotational (<2 degrees) motion (Supporting Information Tables S2 and S3), demonstrating that motion is present and can potentially corrupt images even in short scans (<5 min) acquired on compliant healthy subjects (see Supporting Information Figure S4 for additional example dataset). In the acquisitions with deliberate motion, the range and SD of motion appear comparable between uncorrected and corrected sequences (Supporting Information Tables S2 and S3). These marked levels of both translational (~2 mm) and rotational (>5 degrees) motion resulted in poor and almost unusable image quality without correction (Figure 2B,F). Resultant artifact was markedly reduced with motion correction, enabling visualization of both gray–white differentiation (Figure 2D) and deep-gray and brainstem nuclei (Figure 2H), although some residual artifact remains (see Supporting Information Figure S4 for an additional example dataset).

The quantitative rater analysis confirmed these observations (Supporting Information Table S4). Statistically

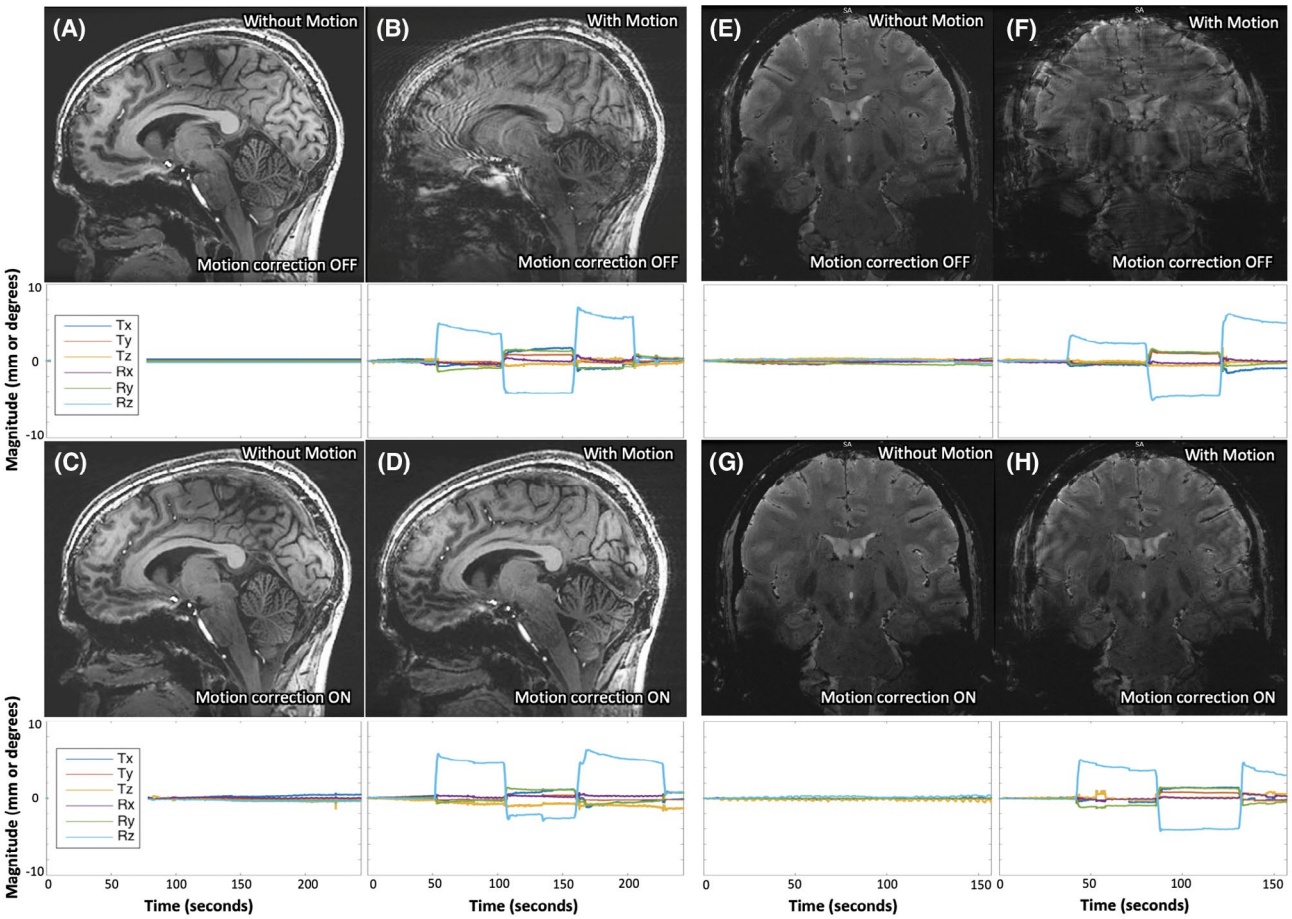

FIGURE 2 Results of 3D IR-FSPGR (A-D) and 2D GRE (E-H) sequences acquired (A and E) without deliberate motion and without motion-correction, (B and F) with deliberate motion and without motion correction, (C and G) without deliberate motion and with motion correction, and (D and H) with deliberate motion and with motion correction on subject 1. Clear improvement of deliberate motion artifact can be seen in the corrected acquisitions (comparing B with D, and F with H). The plots below each image display the translational and rotational motion across time, with the vertical axis showing mm and degrees of displacement or rotation, respectively, and the horizontal showing time in seconds. Each direction of motion was normalized to the subject's initial position for that scan to visualize only net motion during the acquisition. GRE, gradient echo

significant improvements in image quality were seen with motion correction in both acquisitions ($P < .001$), minimally stronger on the 3D-IR-FSPGR acquisitions ($P = .045$). The effect of motion correction was stronger in acquisitions with deliberate motion ($P = .021$). Likewise, for gray–white junction visualization on the 3D-IR-FSPGR acquisitions, ratings were overall worse with motion ($P < .001$) and better with motion correction ($P = .043$), with the effect of motion correction stronger in the presence of motion ($P < .001$). Similarly, for both deep gray nuclei and hippocampal visualization on the 2D-GRE acquisitions, ratings were overall worse with motion ($P < .001$) and better with motion correction ($P < .001$), with the effect of motion correction stronger in the presence of motion ($P = .011$). For all subjects, the PMC-corrected image quality was the same or better on visual rating for 3D-IRFSPGR across the majority of raters for matched motion/no-motion pairs. The same was true for GRE, except for 1 subject with intentional motion in whom the uncorrected GREs was rated a 4 and the corrected GREs a 5 on all metrics (both ratings are unusable for clinical diagnosis). Thus, no acquisitions showed a clinically meaningful worsening with the addition of motion correction.

2. Test 2: The 20-minute ultrahigh-resolution 2D-GRE acquisition showed more than double the range and SD of motion compared to the shorter 4-min acquisitions (Figure 3, Supporting Information Table S5) on the same subject. Both rigid-head and physiological respiratory motion were detected (Figure 3). Motion-corrected images demonstrated exquisite quality despite the long scan time, providing high-resolution visualization of the hippocampus and deep gray nuclei.
3. Test 3: For the serially acquired single average scans, real-time recording of subject position during and between acquisitions provided robust registration across acquisitions without any additional postprocessing (Figure 4) (Supporting Information Table S6). The averaged images are of comparable quality to the longer, 4-average scan, demonstrating the ability of the PMC system to facilitate ultrahigh-resolution scans over shorter, clinically practical time scales (Figure 4).
4. Test 4: At the start of the fifth single average acquisition, following the subject being removed from the bore and stepping off of the table, the subject's initial position was markedly different from the original calibrated position

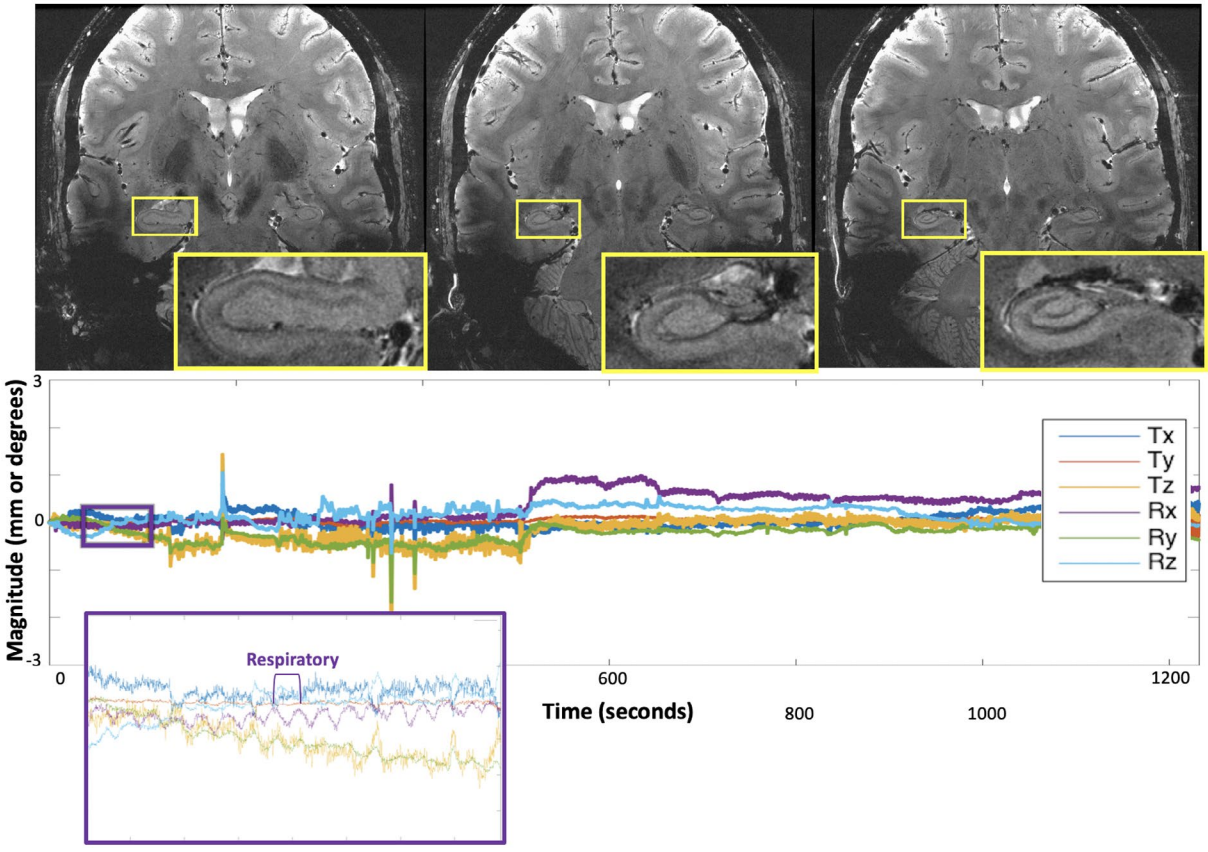

FIGURE 3 Results of the 20-min ultrahigh-resolution 2D GRE sequence, demonstrating exquisite quality imaging of the hippocampus and the remainder of the visualized brain. The plots below each image display the translational and rotational motion across time, with the vertical axis showing mm and degrees of displacement or rotation, respectively, and the horizontal showing time in seconds. Each direction of motion was normalized to the subject's initial position for this scan to visualize only net motion during the acquisition. The purple and orange insets show detection of physiologic respiratory motion, respectively, in addition to rigid-head motion

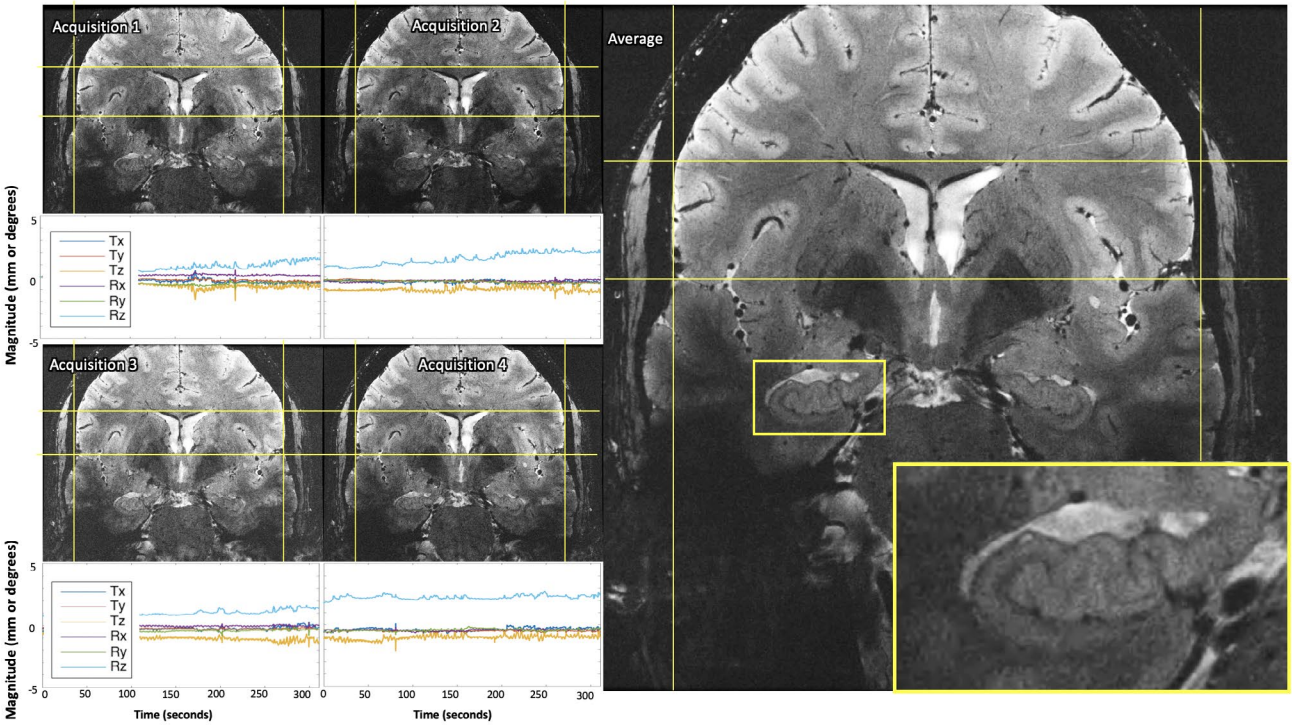

FIGURE 4 Results of serially acquired single average ultrahigh-resolution images (A-D) remained well aligned between acquisitions and comparable quality when averaged (E), despite motion during each scan. The plots below each image display the translational and rotational motion across time, with the vertical axis showing mm and degrees of displacement or rotation, respectively, and the horizontal showing time in seconds. Each direction of motion was normalized to the subject's initial position at the beginning of the first single average ultrahigh-resolution acquisition to visualize net motion during all serial acquisitions

(~2 mm and ~4 degrees), but image quality remained high with images well registered across acquisitions (Figure 5) (Supporting Information Table S6), demonstrating that the system remains effective even when the subject leaves the bore during an exam.

4 | DISCUSSION

In this study, we successfully implemented an optical PMC system for brain imaging at 7T using a custom-built, within-coil camera and head-mounted optical marker for tracking. Using this system, detection of both deliberate and involuntary (rigid-head, respiratory, and cardiac) motion was demonstrated on human subjects, and motion correction produced high-quality images without introducing spurious artifacts. We demonstrated the system's ability to make possible otherwise untenably long scans, enabling ultrahigh-resolution imaging. Finally, we demonstrated that our approach enables robust alignment of serially acquired scans, providing subjects the opportunity to leave the bore between scans while still allowing acquisition of high-fidelity images. The key advantage of PMC in this setting is that we can achieve high SNR using averaging of scans with clinically tractable scan durations without the need for image registration, which can be difficult for slabs with limited coverage and can introduce blurring. Our rater analysis demonstrates that PMC with this system provides significantly improved overall image quality (ie, reduced motion artifact) and allows for better visualization of clinically important structures: the gray–white junction (focal cortical dysplasias[37]), the deep gray nuclei (movement disorders[38]), and the hippocampus (neurodegenerative diseases,[39] epilepsy,[40] and mild traumatic brain injury[41]). The effect of motion correction is seen in healthy, compliant subjects with minimal motion, but a larger improvement is seen in the context of larger magnitude motion. This suggests the system will provide significant benefit when scanning clinical populations who are prone to move during scans, allowing for more nuanced diagnosis and staging of disease and the development of novel biomarkers.

Our approach builds on the work of the Magdeburg group, which pioneered the use of optical prospective motion correction at 7T using a mouthpiece.[25-29] Our within-coil camera provides clear line of sight to the optical marker on the subject's forehead, eliminating the need for the mouthpiece. Mouthpieces are rigidly bound to the upper teeth but remain difficult to implement clinically because they are time consuming to make, less comfortable for patients, make it difficult for patients to communicate with technicians, and are influenced by chewing

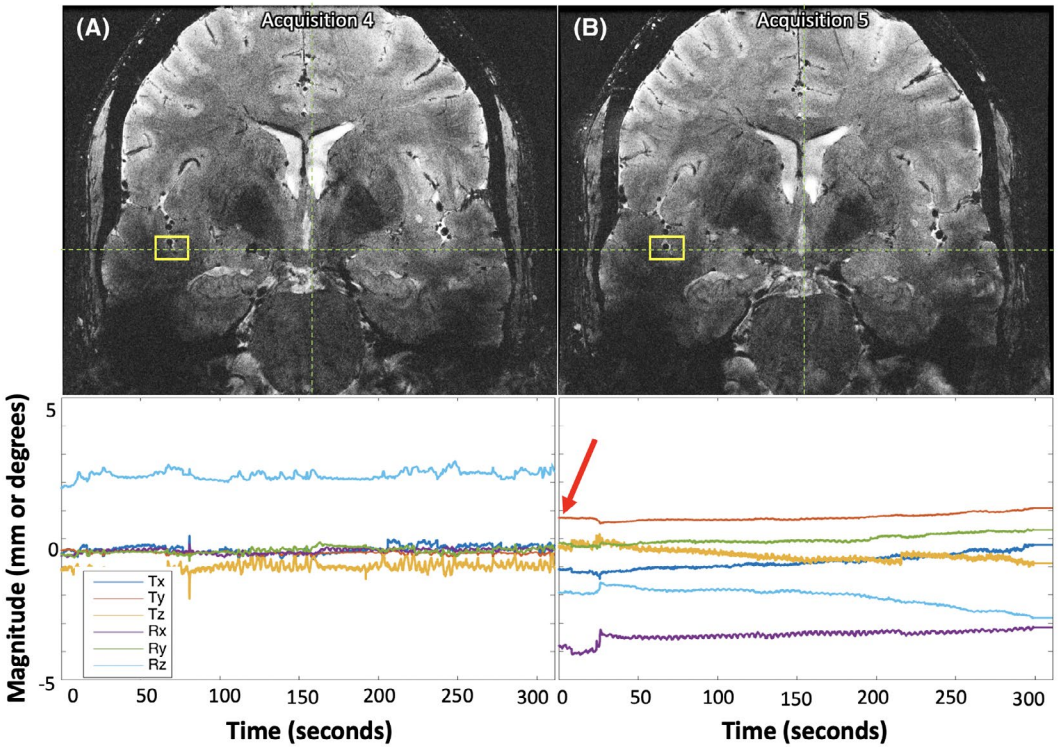

FIGURE 5 Despite the subject being removed from the bore between the fourth (A) and fifth (B) single average ultrahigh-resolution acquisitions and the subject's initial position for the fifth acquisition being noticeably different than the initial calibration point (B, red arrow), the images are well aligned (yellow boxes). The plots below each image display the translational and rotational motion across time, with the vertical axis showing mm and degrees of displacement or rotation, respectively, and the horizontal showing time in seconds. Each direction of motion was normalized to the subject's initial position at the beginning of the first single average ultrahigh-resolution acquisition to visualize net motion during all serial acquisitions

and tongue motion. A limitation of attaching the marker to the forehead is that the skin can move relative to the skull, but the use of medical adhesive (Opsite Flexifix, Smith and Nephew, Watford, UK) placed tightly on the forehead while the skin above the eyebrow is stretched before placement of the marker appears effective at reducing this. Likewise, hair can obscure the view of the marker and needs to be pulled back. Prior to scanning, the only additional step required for technologists is placing the marker on the subject's forehead. The simplicity and comfort of this optical PMC system makes translation to clinical use practical. Whereas under certain scanning conditions the required power is increased with the camera in place, this is at most a ~25% increase, and it is likely that some of this energy is deposited in the camera and not the patient. We do not believe that this increase will be prohibitive for clinically relevant scanning protocols. Our future work will include better characterization and reduction of this increase in required power.

The current system is limited by the latency between the scanner and PMC. Previous studies by our group on earlier camera prototypes and the same marker at 3T showed a latency time of ~24 ms[42]; therefore, very fast motion such as coughing may not be fully corrected and may cause residual motion artifacts. The theoretical limit for latency is based on the frame rate of the camera (in our system, 10 ms given the 100Hz frame rate) plus the time needed to determine marker position (which could be reduced with faster image processing) and update the scanner gradients. Additionally, optical PMC systems correct for real-time changes in the position and orientation of the head within the scanner but not for residual field perturbations, which could still cause artifacts. Another limitation of this experimental prototype is that the power supply is an external battery with finite charge, limiting the length of protocols that currently can be performed in a single sitting. Finally, the current prototype of this system has the camera mounted to the same location where mirrors are mounted for task-based functional imaging, meaning this system cannot be used during protocols with visual stimuli. Alternative camera mounting designs that would provide a line of sight to a bite bar marker could also be envisioned.

The presented results should be interpreted within the limitations of this study. To compare the effect of motion correction on image quality, scans were repeated sequentially with and without motion correction. Although subjects' deliberate motion cannot be entirely identical between repetitions of sequences, the quantitative motion tracking data measured here shows similar magnitudes and frequency of motion between scans. Moreover, the motion conditions tested in this study were of compliant, healthy subjects either

holding as still as possible or making exaggerated motions. It is possible that the motion produced by clinical subjects may differ. This should be considered when translating to clinical populations. Moreover, we have tested our system on only 2 specific sequences in this paper. Ongoing work aims to extend these PMC methods to additional sequences, including multi-echo sequences, EPI, and high-resolution T_1-weighted sequences, to confirm that the conclusions of this study can be applied to additional sequences relevant for 7T brain exams. Future work should also include quantitative assessment of image quality in addition to the rater analysis already performed.

5 | CONCLUSION

This work demonstrates that this optical PMC system may overcome motion artifact in brain imaging at 7T, one of the biggest challenges precluding utilization of ultrahigh-field MR in both research and clinical settings. This practical, user-friendly design allows longer scan times and finer image resolution, providing potential to facilitate the discovery of novel biomarkers of aging and disease.

ACKNOWLEDGMENT

The authors would like to acknowledge research support by GE Healthcare (Chicago, IL), National Institutes of Health (NIH) P41 EB015891, NIH S10 RR026351-01A1, NIH R01 AG061120-01, and the American Society of NeuroRadiology Boerger Alzheimer's Fund. The authors would also like to thank Nicole Mouchawar for her assistance with manuscript preparation.

CONFLICT OF INTEREST

The authors of this manuscript are listed as inventors on numerous patents and patent applications relating to motion correction in MRI. Drs. Aksoy, Bammer, and Maclaren consult for HobbitView Inc. (San Jose, CA), a company that aims to commercialize motion correction methods.

ORCID

Phillip DiGiacomo https://orcid.org/0000-0002-2441-4086

REFERENCES

1. De Reuck J, Deramecourt V, Auger F, et al. Post-mortem 7.0-Tesla magnetic resonance study of cortical microinfarcts in neurodegenerative diseases and vascular dementia with neuropathological correlates. *J Neurol Sci*. 2014;346:85–89.
2. Yao B, Hametner S, van Gelderen P, et al. 7-Tesla magnetic resonance imaging to detect cortical pathology in multiple sclerosis. *PLoS ONE*. 2014;9:e108863.
3. Zucca I, Milesi G, Medici V, et al. Type II focal cortical dysplasia: ex vivo 7T magnetic resonance imaging abnormalities and histopathological comparisons. *Ann Neurol*. 2016;79:42–58.
4. Kenkhuis B, Jonkman LE, Bulk M, et al. 7T MRI allows detection of disturbed cortical lamination of the medial temporal lobe in patients with Alzheimer's disease. *Neuroimage Clin*. 2019;21:101665.
5. Deistung A, Schäfer A, Schweser F, Biedermann U, Turner R, Reichenbach JR. Toward in vivo histology: a comparison of quantitative susceptibility mapping (QSM) with magnitude-, phase-, and $R2_*$-imaging at ultra-high magnetic field strength. *Neuroimage*. 2013;65:299–314.
6. Bianciardi M, Strong C, Toschi N, et al. A probabilistic template of human mesopontine tegmental nuclei from in vivo 7T MRI. *Neuroimage*. 2018;170:222–230.
7. Muckli L, De Martino F, Vizioli L, et al. Contextual feedback to superficial layers of V1. *Curr Biol*. 2015;25:2690–2695.
8. de Graaf WL, Zwanenburg JJ, Visser F, et al. Lesion detection at seven Tesla in multiple sclerosis using magnetisation prepared 3D-FLAIR and 3D-DIR. *Eur Radiol*. 2012;22:221–231.
9. van Veluw SJ, Zwanenburg JJM, Engelen-Lee J, et al. In vivo detection of cerebral cortical microinfarcts with high-resolution 7T MRI. *J Cereb Blood Flow Metab*. 2013;33:322–329.
10. Harrison DM, Roy S, Oh J, et al. Association of cortical lesion burden on 7-T magnetic resonance imaging with cognition and disability in multiple sclerosis. *JAMA Neurol*. 2015;72:1004–1012.
11. De Ciantis A, Barba C, Tassi L, et al. 7T MRI in focal epilepsy with unrevealing conventional field strength imaging. *Epilepsia*. 2016;57:445–454.
12. Obusez EC, Lowe M, Oh SH, et al. 7T MR of intracranial pathology: preliminary observations and comparisons to 3T and 1.5 T. *Neuroimage*. 2019;168:459–476.
13. Shah P, Bassett DS, Wisse LE, et al. Structural and functional asymmetry of medial temporal subregions in unilateral temporal lobe epilepsy: a 7T MRI study. *Hum Brain Mapp*. 2019;40:2390–2398.
14. Uğurbil K, Auerbach E, Moeller S, et al. Brain imaging with improved acceleration and SNR at 7 Tesla obtained with 64-channel receive array. *Magn Reson Med*. 2019;82:495–509.
15. Gallichan D, Marques JP, Gruetter R. Retrospective correction of involuntary microscopic head movement using highly accelerated fat image navigators (3D FatNavs) at 7T. *Magn Reson Med*. 2016;75:1030–1039.
16. Engström M, Mårtensson M, Avventi E, Norbeck O, Skare S. Collapsed fat navigators for brain 3D rigid body motion. *Magn Reson Imaging*. 2015;33:984–991.
17. Gallichan D, Marques JP. Optimizing the acceleration and resolution of three-dimensional fat image navigators for high-resolution motion correction at 7T. *Magn Reson Med*. 2017;77:547–558.
18. Federau C, Gallichan D. Motion-correction enabled ultra-high resolution in-vivo 7T MRI of the brain. *PLoS One*. 2016;11:e0154974.
19. Ooi MB, Krueger S, Thomas WJ, Swaminathan SV, Brown TR. Prospective realtime correction for arbitrary head motion using active markers. *Magn Reson Med*. 2009;62:943-954.
20. Haeberlin M, Kasper L, Barmet C, et al. Realtime motion correction using gradient tones and head-mounted NMR field probes. *Magn Reson Med*. 2014;74:647–660.
21. Vannesjo SJ, Wilm BJ, Duerst Y, et al. Retrospective correction of physiological field fluctuations in high-field brain MRI using concurrent field monitoring. *Magn Reson Med*. 2015;73:1833–1843.
22. White N, Roddey C, Shankaranarayanan A, et al. PROMO: real-time prospective motion correction in MRI using image-based tracking. *Magn Reson Med*. 2010;63:91–105.
23. Schulz J, Siegert T, Reimer E, et al. An embedded optical tracking system for motion-corrected magnetic resonance imaging at 7T. *MAGMA*. 2012;25:443–453.

24. Maclaren J, Armstrong BSR, Barrows RT, et al. Measurement and correction of microscopic head motion during magnetic resonance imaging of the brain. *PLoS One*. 2012;7:e48088.
25. Stucht D, Danishad KA, Schulze P, Godenschweger F, Zaitsev M, Speck O. Highest resolution in vivo human brain MRI using prospective motion correction. *PLoS One*. 2015;10:e0133921.
26. Mattern H, Sciarra A, Godenschweger F, et al. Prospective motion correction enables highest resolution time-of-flight angiography at 7T. *Magn Reson Med*. 2018;80:248–258.
27. Mattern H, Sciarra A, Lüsebrink F, Acosta-Cabronero J, Speck O. Prospective motion correction improves high-resolution quantitative susceptibility mapping at 7T. *Magn Reson Med*. 2019;81:1605–1619.
28. Zaitsev M, Dold C, Sakas G, Hennig J, Speck O. Magnetic resonance imaging of freely moving objects: prospective real-time motion correction using an external optical motion tracking system. *Neuroimage*. 2006;31:1038–1050.
29. Speck O, Hennig J, Zaitsev M. Prospective real-time slice-by-slice motion correction for fMRI in freely moving subjects. *MAGMA*. 2006;19:55–61.
30. Maclaren J, Aksoy M, Ooi MB, Zahneisen B, Bammer R. Prospective motion correction using coil-mounted cameras: cross-calibration considerations. *Magn Reson Med*. 2018;79:1911–1921.
31. Spangler-Bickell MG, Khalighi MM, Hoo C, et al. Rigid motion correction for brain PET/MR imaging using optical tracking. *IEEE Trans Radiat Plasma Med Sci*. 2019;3:498–503.
32. DiGiacomo PS, Tong E, Maclaren J, et al. A novel, coil-integrated camera for prospective optical motion correction of brain imaging at 7T. In Proceedings of the 27th Annual Meeting of ISMRM, Montréal, Québec, Canada, 2019. Abstract 4436.
33. Forman C, Aksoy M, Hornegger J, Bammer R. Self-encoded marker for optical prospective head motion correction in MRI. *Med Image Anal*. 2011;15:708–719.
34. Tanenbaum LN, Tsiouris AJ, Johnson AN, et al. Synthetic MRI for clinical neuroimaging: results of the magnetic resonance image compilation (MAGiC) prospective, multicenter, multireader trial. *Am J Neuroradiol*. 2017;38:1103–1110.
35. Zeineh M, Parekh M, Zaharchuk G, et al. Ultra-high resolution imaging of the human brain with phase-cycled balanced steady state free precession at 7.0 T. *Invest Radiol*. 2014;49:278–289.
36. StataCorp. *Stata Statistical Software: Release 15*. College Station, TX: StataCorp LLC; 2017.
37. Blackmon K, Kuzniekcy R, Barr WB, et al. Cortical gray-white matter blurring and cognitive morbidity in focal cortical dysplasia. *Cereb Cortex*. 2015;25:2854–2862.
38. Telford R, Vattoth S. MR anatomy of deep brain nuclei with special reference to specific diseases and deep brain stimulation localization. *Neuroradiol J*. 2014;27:29–43.
39. Den Heijer T, van der Lijn F, Koudstaal PJ, et al. A 10-year follow-up of hippocampal volume on magnetic resonance imaging in early dementia and cognitive decline. *Brain*. 2010;133:1163–1172.
40. Santyr BG, Goubran M, Lau JC, et al. Investigation of hippocampal substructures in focal temporal lobe epilepsy with and without hippocampal sclerosis at 7T. *J Magn Reson Imaging*. 2017;45:1359–1370.
41. Parivash S, Goubran M, Mills BD, et al. Longitudinal changes in hippocampal subfield volume associated with collegiate football. *J Neurotrama*. 2019;36:2762–2773.
42. Maclaren J. Ooi MB, Aksoy M, Ehrl J, Bammer R. Calibration and quality assurance for optical prospective motion correction using active markers. In Proceedings of the 22nd Annual Meeting of ISMRM, Milan, Italy, 2014. Abstract 4340.

SUPPORTING INFORMATION

Additional Supporting Information may be found online in the Supporting Information section.

FIGURE S1 Schematic of (A) camera housing, showing power and fiber connections, and (B) camera rig, which allows camera to be mounted on the receive part of the 7T head coil

FIGURE S2 Echo planar imaging (EPI) phantom validation study shows no conspicuous difference between the variance maps acquired without (A) and with (B) the camera and battery installed, confirming that the hardware does not impact temporal stability. The difference maps computed for magnitude (C,D) and variance (E,F) images between the with and without camera acquisitions (C,E) show similar magnitude to those from duplicate acquisitions without the camera (D,F). Note, this experiment utilized a 19 cm diameter agar gel phantom, placed in the coil such that it is ~5 cm from the camera, similar to the distance between the camera and an adult human head. These images were windowed and leveled identically

FIGURE S3 Phantom validation study shows artifact from deliberate motion without correction (A), significantly improved after correction (B). The plots below each image display the translational and rotational motion across time, with the vertical axis showing mm and degrees of displacement or rotation, respectively, and the horizontal showing time in seconds. Each direction of motion was normalized to the papaya's initial position for that scan, to visualize only net motion during the acquisition. Motion is best seen on the blue trace at a frequency of approximately 0.2 Hz

FIGURE S4 Results of 3D IRFSPGR (A-D) and 2D GRE sequences (E-H) sequences acquired (A and E) without deliberate motion and without motion-correction, (B and F) with deliberate motion and without motion-correction, (C and G) without deliberate motion and with motion-correction, and (D and H) with deliberate motion and with motion-correction on Subject 2. The plots below each image display the translational and rotational motion across time, with the vertical axis representing both mm and degrees of displacement, and the horizontal representing seconds. Each direction of motion was normalized to the subject's initial position for that scan, to visualize only net motion during the acquisition. Note the *y*-axis is from −15 to 15 for A-D and −20 to 20 for E-H

TABLE S1 Sequence parameters for the *in vivo* MRI scans acquired in this study

TABLE S2 Quantification of motion in each direction by Subject 1 during 3D IR-FSPGR MRI scans. Despite the subject being asked to hold still, modest levels of translational and rotational motion are observed across scans. Note: SD = standard deviation; translations are in mm; rotations are in degrees

TABLE S3 Quantification of motion in each direction by Subject 1 during 2D GRE MRI scans. Note: SD = standard deviation; translations are in mm; rotations are in degrees

TABLE S4 Results of the visual rater analysis. Mean and confidence intervals for each rating scale across each condition

TABLE S5 Quantification of motion in each direction by Subject 1 during 4 average ultra-high-resolution 2D GRE MRI scan. Compared to the shorter, regular resolution scans, we see higher ranges and standard deviations of motion. Note: SD = standard deviation; translations are in mm; rotations are in degrees

TABLE S6 Quantification of motion in each direction by Subject 1 during single average ultra-high-resolution 2D GRE MRI scans. Note: SD = standard deviation; translations are in mm; rotations are in degrees

How to cite this article: DiGiacomo P, Maclaren J, Aksoy M, et al. A within-coil optical prospective motion-correction system for brain imaging at 7T. *Magn Reson Med*. 2020;00:1–11.
https://doi.org/10.1002/mrm.28211